The Electronic Supplementary Information for

Aggregation-induced Emission Active Thermally-activated Delayed Fluorescence Materials Possessing *N*-Heterocycle and Sulfonyl Groups

Yasunori Matsui,[ab]* Yudai Yokoyama,[a] Takuya Ogaki,[ab] Kenta Ishiharaguchi,[c] Akitsugu Niwa,[c] Eisuke Ohta,[ab] Masaki Saigo,[d] Kiyoshi Miyata,[d] Ken Onda,[d]* Hiroyoshi Naito,[bc]* and Hiroshi Ikeda[ab]*

[a] Department of Applied Chemistry, Graduate School of Engineering, Osaka Prefecture University, 1-1 Gakuen-cho, Naka-ku, Sakai, Osaka 599-8531, Japan
[b] The Research Institute for Molecular Electronic Devices (RIMED), Osaka Prefecture University, 1-1 Gakuen-cho, Naka-ku, Sakai, Osaka 599-8531, Japan
[c] Department of Physics and Electronics, Graduate School of Engineering, Osaka Prefecture University, 1-1 Gakuen-cho, Naka-ku, Sakai, Osaka 599-8531, Japan
[d] Department of Chemistry, Graduate School of Science, Kyushu University, 774 Motooka, Nishi-ku, Fukuoka 819-0395, Japan

Table of Contents

1. General

Melting points (mp) were obtained with a Yanaco MP-500 or a Rigaku Thermo plus 2 EVO and are reported uncorrected. ^{1}H and ^{13}C NMR spectra were recorded at 400 and 100 MHz, respectively, on a Bruker AVANCE NEO 400 spectrometer. Chemical shifts (δ) are reported in ppm using the signal of tetramethylsilane (0.00 ppm) and $CDCl_3$ (77.00 ppm) as an internal standard for ^{1}H and ^{13}C NMR, respectively. IR spectra were recorded on a JASCO FT/IR 8300 spectrometer with transmission or attenuated total reflection (ATR) method. Low-resolution (LR) atmospheric solid analysis probe (ASAP) mass measurements were carried out with a Shimadzu LCMS-2020 and LabSolutions LCMS software. High-resolution (HR) electrospray ionization (ESI) mass measurements were carried out on a Bruker micrOTOF system after calibration using a sodium formate solution. Elemental analyses were carried out at the Research and Analytical Centre at Kanazawa University. UV–Vis absorption and photoluminescence (PL) spectra were recorded on JASCO V-570 and FP-8500 spectrophotometers, respectively. Absolute PL quantum yields were determined by utilizing the integrating sphere method with a HAMAMATSU C9920-02 absolute PL quantum yields measurement system. PL decay profiles for solutions were measured by using a HORIBA Jobin Yvon FluoroCube lifetime spectrofluorometer and analyzed using DAS6 PL decay analysis software. PL decay profiles for solid samples were measured by using a polychromator and a streak camera system (Hamamatsu C4780, time resolution: < 30 ps) synchronized with a regenerative Ti:sapphire amplifier (Spitfire Ace, ~120 fs, 1 kHz, 4 mJ/pulse, 800 nm). The output of the amplifier was led to the optical parametric amplifier (Spectra-Physics, TOPAS-prime), and the fourth harmonic wave (365 nm, < 21 μJ/cm^2) of the signal pulse was used for excitation. All materials and solvents were used as purchased, unless otherwise noted.

2. Preparation of Substrates

Synthesis of 2Cz2SB and 2Mi2SB was carried out according to Scheme 1 in the main text. The detail of conversion of 1,2,4,5-tetrafluorobenzene using KSC_6H_4-^{t}Bu to **2** is as follows. The final step reactions of **2** to give 2Cz2SB and 2Mi2SB were described in the experimental section of the main text.

Potassium 4-(*tert*-butyl)benzenethiolate (KSC_6H_4-^{t}Bu): To a 200-mL round-bottom flask, 4-*tert*-butylbenzenethiol (5.0 g, 30 mmol), KOH (1.65 g, 25 mmol), and benzene (100 mL) were added and stirred for 5 h at 80 °C. After cooling to room temperature, precipitated solid was filtrated and washed by *n*-hexane (20 mL). Drying under reduced pressure gave

KSC_6H_4-^{t}Bu as a colourless powder (5.02 g, 24.6 mmol, y. 98%). mp > 300 °C; ^{1}H NMR (400 MHz, DMSO-d_6) δ_{ppm} 1.31 (s, 9H), 7.37 (AA'XX', J = 8.4 Hz, 2H), 7.45 (AA'XX', J = 8.4 Hz, 2H); ASAP-mass m/z 165 ($C_{10}H_{13}S^-$).

1,4-Difluoro-2,5-bis((4-*tert*-butyl)phenylthio)benzene (1): To a three-necked round-bottom flask, KSC_6H_4-^{t}Bu (4.09 g, 20 mmol) and pyridine (40 mL) were added and stirred at 120 °C under Ar atmosphere. After 15 min, a pyridine solution of 1,2,4,5-tetrafluorobenzene (1.20 g, 8 mmol) was added dropwise and stirred at 120 °C for 16 h. After cooling to room temperature, the reaction mixture was poured into ice-water. Recrystallization of the precipitated solid from benzene gave **1** as colourless needles (2.54 g, 5.8 mmol, y. 72%). mp 167–169 °C; ^{1}H NMR (400 MHz, $CDCl_3$) δ_{ppm} 1.33 (s, 18H), 6.73 (t, J = 7.6 Hz, 2H), 7.35 (AA'BB', J = 8.7 Hz, 4H), 7.39 (AA'BB', J = 8.7 Hz, 4H); ^{13}C NMR (100 MHz, $CDCl_3$) δ_{ppm} 31.2 (6C), 34.7 (2C), 117.2 (dd, J^{CF} = 18.9, 10.0 Hz, 2C), 124.5 (dd, J^{CF} = 15.7, 12.6 Hz, 2C), 126.8 (4C), 127.9 (2C), 132.8 (4C), 152.0 (2C), 155.9 (dd, J^{CF} = 243, 3.7 Hz, 2C); ASAP-mass m/z = 443 ($(M+H)^+$, $C_{26}H_{29}F_2S_2$), Anal. Calcd. for $C_{26}H_{28}F_2S_2$: C, 71.65; H, 6.80. Found: C, 71.94; H, 6.85.

1,4-Difluoro-2,5-bis((4-*tert*-butyl)phenylsulfonyl)benzene (2): To a round-bottom flask, **1** (1.77 g, 4.0 mmol), 3-chloroperbenzoic acid (*m*CPBA, 5.55 g, 21 mmol), CH_2Cl_2 (80 mL) were added and stirred for 21 h at room temperature. After addition of 20% aqueous NaOH (100 mL), the solution was extracted by CH_2Cl_2 (100 mL × 2). The combined extracts were washed with saturated aqueous NaCl and concentrated under reduced pressure. Recrystallization of the obtained solid from $CHCl_3$–*n*-hexane gave **2** as colourless powder. mp > 300 °C; ^{1}H NMR (300 MHz, $CDCl_3$) δ_{ppm} 1.33 (s, 18H), 7.57 (AA'BB', J = 8.4, 4H), 7.85 (t, J = 7.2 Hz, 2H), 7.91 (AA'BB', J = 8.4 Hz, 4H); ^{13}C NMR (100 MHz, $CDCl_3$) δ_{ppm} 31.0 (6C), 35.4 (2C), 118.8 (dd, J^{CF} = 17.5, 10.1 Hz, 2C), 126.6 (4C), 128.5 (4C), 135.1–136.2 (m, 2C+2C), 154.4 (dd, J^{CF} = 259, 5.1 Hz), 158.9 (2C); IR (ATR) ν/cm^{-1} 1592, 1467, 1387, 1332, 1295, 1190, 1164, 1113, 1093, 902, 831, 797, 754, 674; Anal. Calcd. for $C_{26}H_{28}F_2O_4S_2$: C, 61.64; H, 5.57. Found: C, 60.81; H, 5.50. HR-MS (ESI+) m/z = 507.1469 (Calcd. for $C_{26}H_{29}F_2S_2O_4$ $(M+H)^+$, 507.1470).

3. Crystal Packing Structure of 2Cz2SB

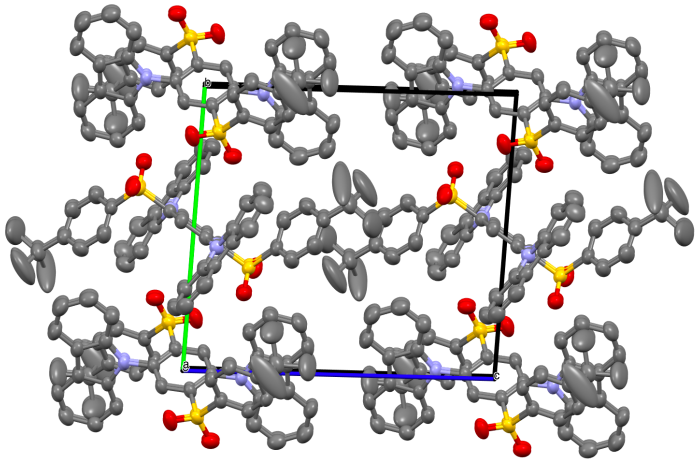

Fig. S1. Crystal packing diagram of 2Cz2SB. No remarkable attractive interactions are observed between the neighbouring molecules.

4. Determination of Excited State Energy Levels

Determination of excited state energy levels of 2Cz2SB and 2Mi2SB was carried out using steady-state PL and delayed (30 ms) PL spectra in 2-MTHF matrices at 77 K (Fig. S2). Analysis of these spectra shows that ΔE_{ST} of 2Cz2SB and 2Mi2SB are 0.02 and 0.09 eV, respectively.

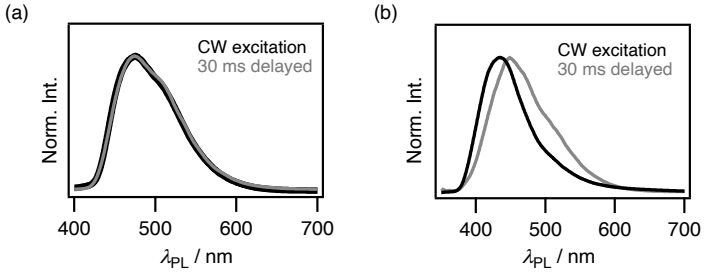

Fig. S2. Steady-state PL (black) and delayed PL (gray, 30 ms) spectra of (a) 2Cz2SB and (b) 2Mi2SB in 2-methyltetrahydrofuran matrix at 77 K.

5. Physical Properties of 2Cz2SB

Table S1. Photophysical Properties of 2Cz2SB in Benzene

λ_{FL} / nm	$\Phi_{PL,air}$	$\Phi_{PL,Ar}$	$\tau_{PL,air}$ / ns	$\tau_{PL,Ar}$ / ns	k_{ISC} / 10^7 s^{-1}	k_{RISC} / 10^5 s^{-1}
524	0.10	0.28	17.6 (89%) 395 (11%)	25.3 (37%) 8820 (63%)	3.4	1.2

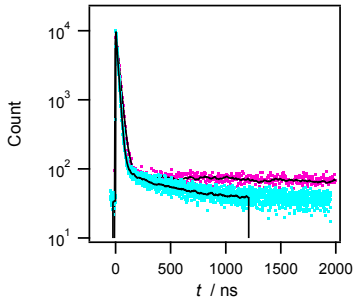

Fig. S3. FL decay profiles of 2Cz2SB in aerated (light blue) and Ar-saturated (purple) benzene.

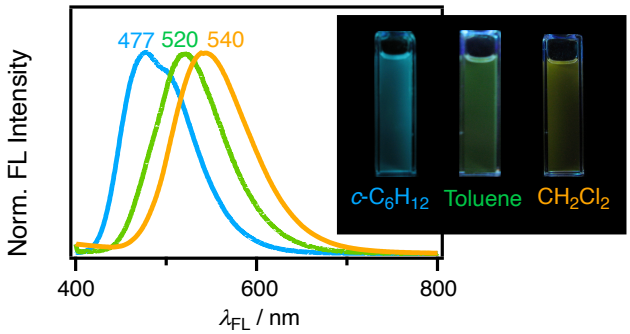

Fig. S4. Fluorescence spectra of 2Cz2SB in degassed c-C_6H_{12}, toluene, and CH_2Cl_2.

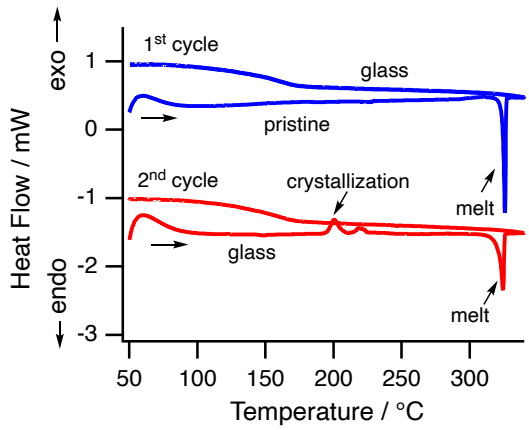

Fig. S5. DSC traces of crystals of 2Cz2SB (scan rate: 5 °C min^{-1}). Exothermic peaks assigned to melting point (325 °C) was observed repeatedly. Also, any remarkable peaks were not observed in the region lower than the melting point at the first cycle, suggesting that 2Cz2SB have a high thermal stability.

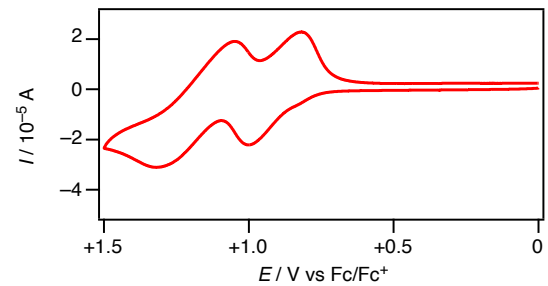

Fig. S6. Cyclic voltammogram of 2Cz2SB (1 mM) in CH_2Cl_2 solution containing $^nBu_4N^+BF_4^-$ (0.1 M). Working and counter electrodes: Pt; Reference electrode: Ag/Ag^+. Sweep rate: 0.1 V s^{-1}. Pseudo-reversible oxidation waves were observed at anodic peak potentials at +1.00 and +1.31 V vs Fc/Fc^+.

6. Numerical Simulations for Population of Excited Species

Populations of S_1- and T_1-excited species were simulated according to the kinetic model shown in Fig. S7. Populations of S_1- and T_1-excited species are described by eqns S1 and S2. As a result, time-dependent population of S_1- and T_1-excited species of 2Cz2SB are depicted in Fig. S8.

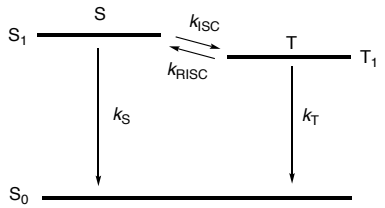

Fig. S7. Kinetic model for deactivation of S_1- and T_1-excited species.

$$\frac{d[\mathrm{S}]}{dt} = -(k_\mathrm{S} + k_\mathrm{ISC})[\mathrm{S}] + k_\mathrm{RISC}[\mathrm{T}] \qquad \text{(S1)}$$

$$\frac{d[\mathrm{T}]}{dt} = k_\mathrm{ISC}[\mathrm{S}] - (k_\mathrm{RISC} + k_\mathrm{T})[\mathrm{T}] \qquad \text{(S2)}$$

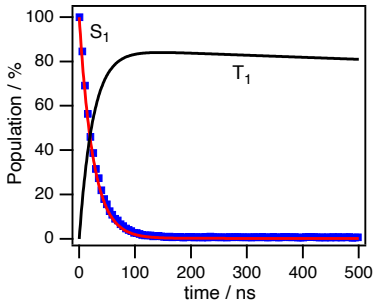

Fig. S8. Population of S_1-(red) and T_1 (black)-excited species of 2Cz2SB in benzene using eqns S1 and S2 with parameters listed in Table S1. Blue dots are experimental FL decay profile.

7. Fabrication of Inverted OLED and Device Characterization

Inverted OLED of 2Cz2SB were fabricated by the following solution process. On the aluminium-doped zinc oxide electrode (cathode), ethanol solution of polyethyleneimine (PEI, 0.05 wt%) was spincoated (2000 rpm, 30 s) to form a PEI layer. After drying, emission layer (2Cz2SB/PMMA = 70/30, 1wt% in CH_2Cl_2) was spincoated (500 rpm, 5 s to 2000 rpm, 60 s). After drying, MoO_3 and Al were vacuum-deposited as a hole-injection layer and anode, respectively. *J–L–V* characteristics and current efficiency are displayed in Figs. S9a and S9b, respectively.

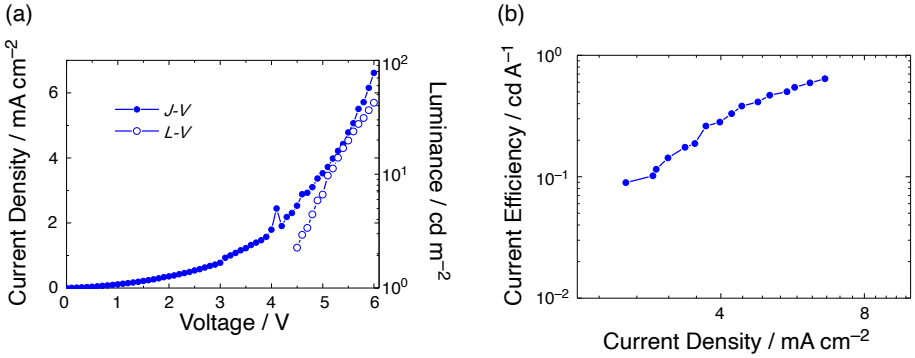

Fig. S9. (a) *J–L–V* characteristics of the fabricated OLED. The maximum luminance was 42 cd m^{-2} at 6 V. (b) Plots of current efficiency against current density. The maximum current efficiency was 0.64 cd A^{-1} at 6 V.

8. Full description of TR-IR Spectra

TR-IR measurements were performed using home-built setups with pump-probe scheme. A broadband mid-IR pulse for a probe light (pulse duration: 120 fs, bandwidth: 150 cm^{-1}, tunable range: 1000–4000 cm^{-1}) was generated by difference-frequency generation between the signal and idler light from an optical parametric amplifier seeded by the output of a Ti:sapphire regenerative amplifier (pulse duration: 120 fs, wavelength: 800 nm, Spitfire Ace, Spectra-Physics). The pump pulse (pulse duration: 6 ns, wavelength: 355 nm) was obtained by third harmonic generation of the output of a nanosecond Nd:YAG laser (EKSPLA NL220). The time delay between the pump and probe pulses was controlled using a digital delay/pulse generator (Stanford Research Systems, DG645). The pump pulse fluence was approximately 2.6 and

26 mJ/cm^2 for KBr pellet and benzene solution, respectively. The sample solutions were continuously circulated through a home-built IR cell equipped with BaF_2 windows with an optical path length of 0.1 mm. A probe pulse passed through the IR cell was dispersed by a 19 cm polychromator, followed by detection using a 64-channel mercury cadmium telluride IR detector array. All measurements in 0.9 mM benzene solutions were performed after 1-h N_2-prebubbling and while bubbling maintained. For the measurement of KBr pellets, the samples were prepared by mixing 2 mg of compounds and 100 mg of ground KBr and pressing it in a die, forming a pellet with diameter of 13.0 mm and thickness of 0.5 mm. The details were given in the previous reports.[46,47,57]

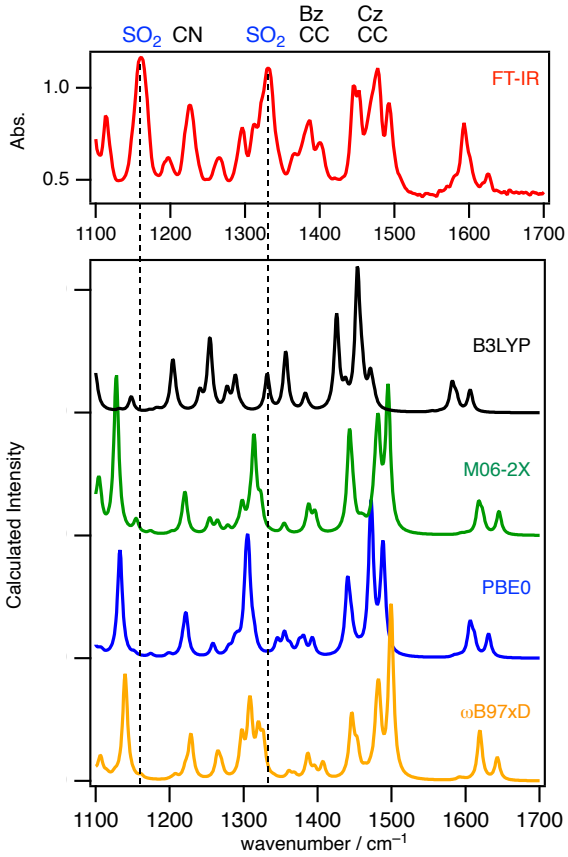

Fig. S10. Correspondence of FT-IR spectrum of 2Cz2SB in a KBr pellet with calculated IR spectra using B3LYP, M06-2X, PBE0, and ωB97xD functionals with 6-31G(d,p) basis set. Scaling factors for all the calculated spectra are 0.96. The M06-2X and PBE0 functionals were suitable for 2Cz2SB.

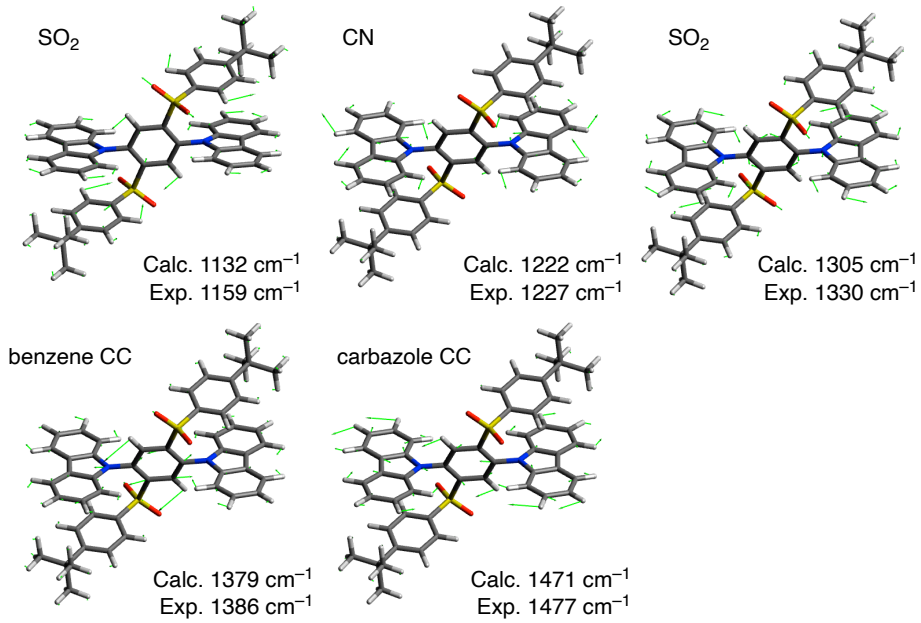

Fig. S11. Assignments for the IR spectrum of 2Cz2SB using the results of calculations at the PBE0/6-31G* level of theory (Scaling factor: 0.96).

9. Quantum Chemical Calculations

The Cartesian coordinates of the optimized geometries are available online as .xyz file.

(a)

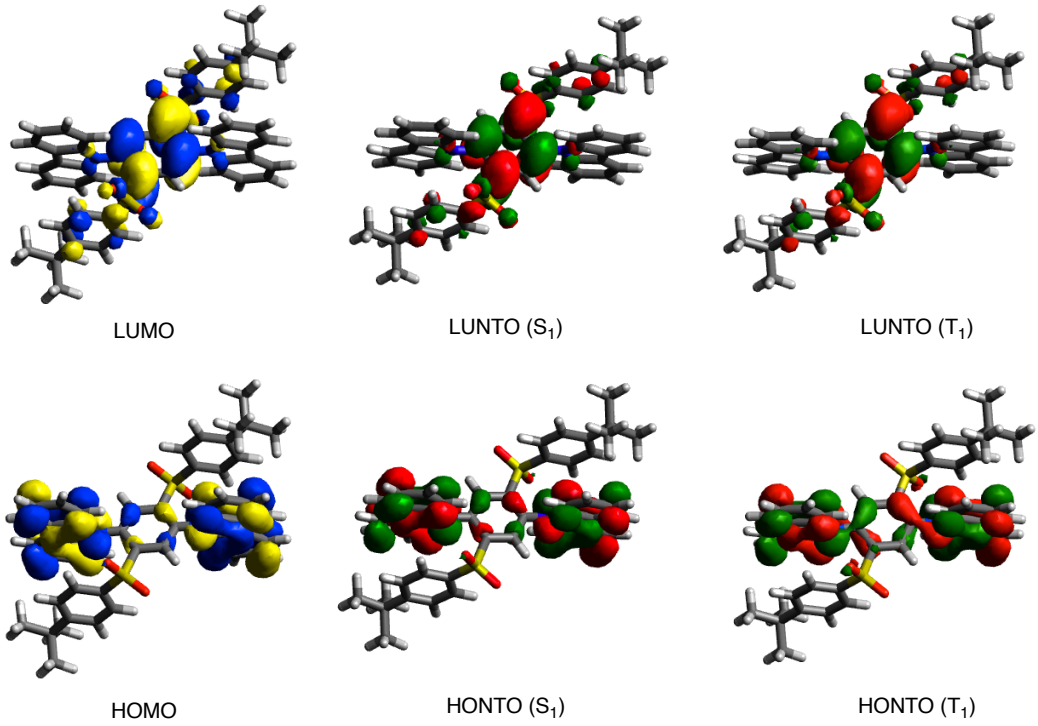

(b)

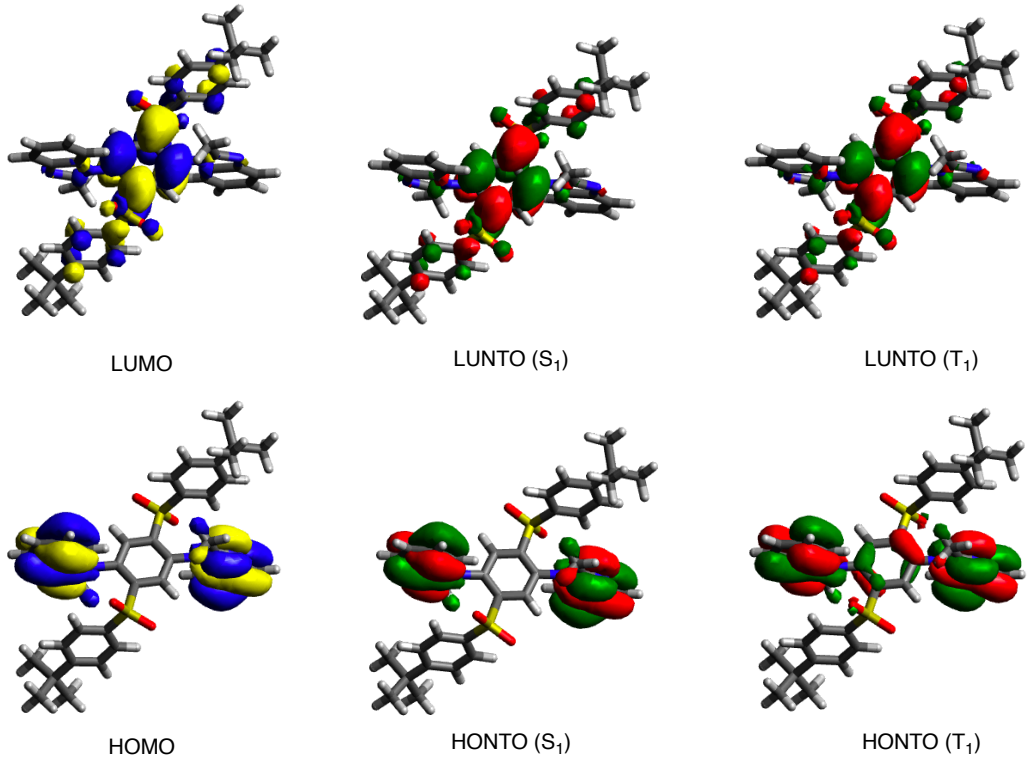

Fig. S12. Frontier molecular orbitals and natural transition orbitals (T_1 and S_1) of (a) 2Cz2SB and (b) 2Mi2SB (B3LYP/6-31G(d,p)).

10. NMR Spectra

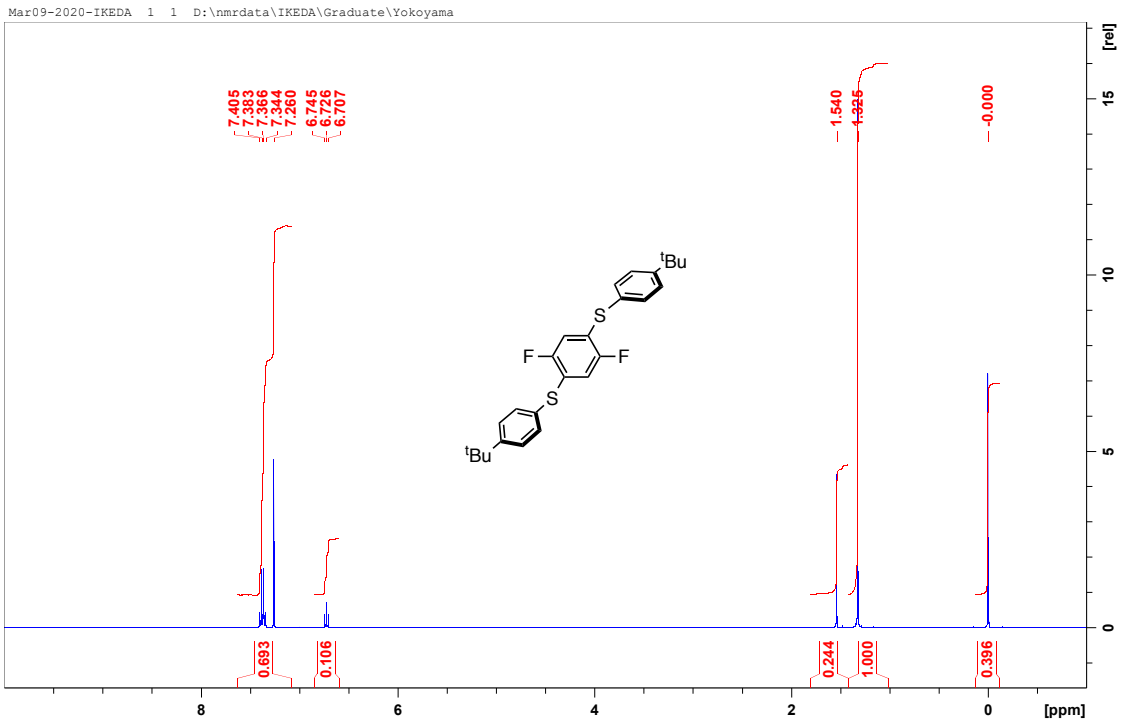

Fig. S13. ^{1}H NMR spectrum of **1** (400 MHz, $CDCl_3$).

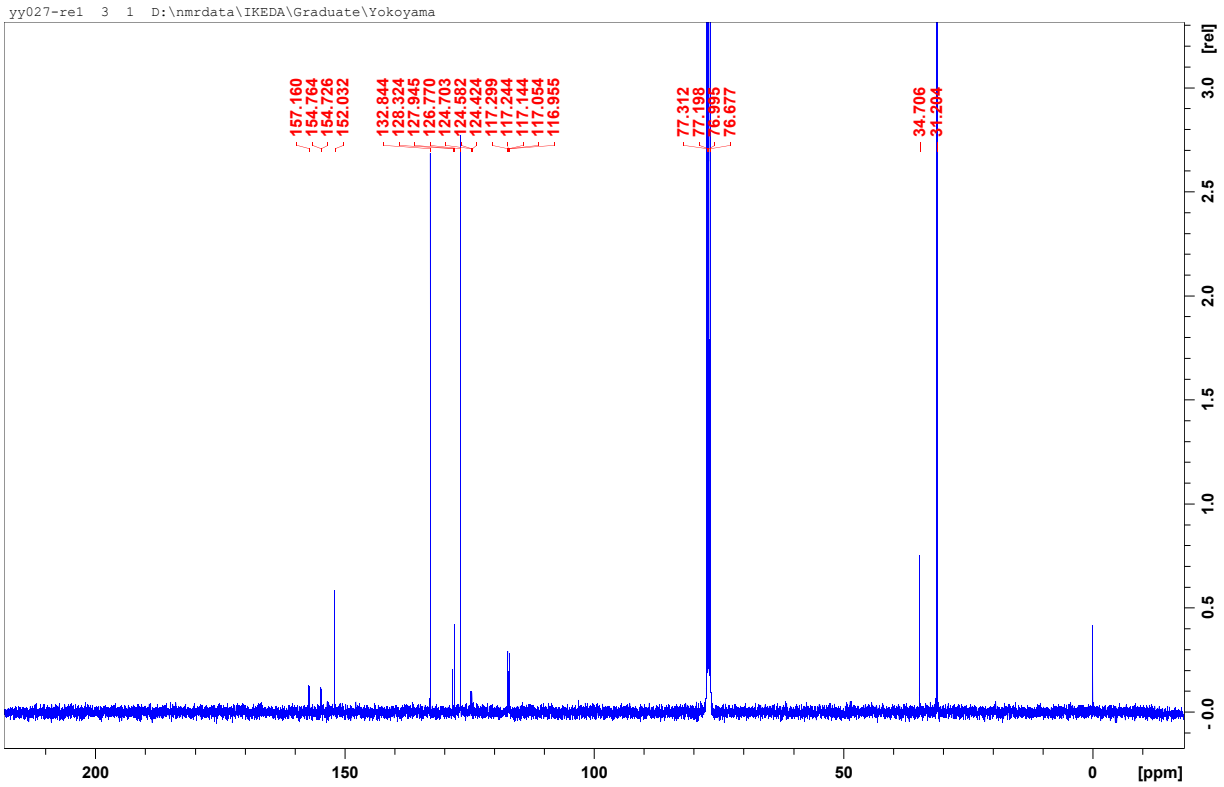

Fig. S14. ^{13}C NMR spectrum of **1** (100 MHz, $CDCl_3$).

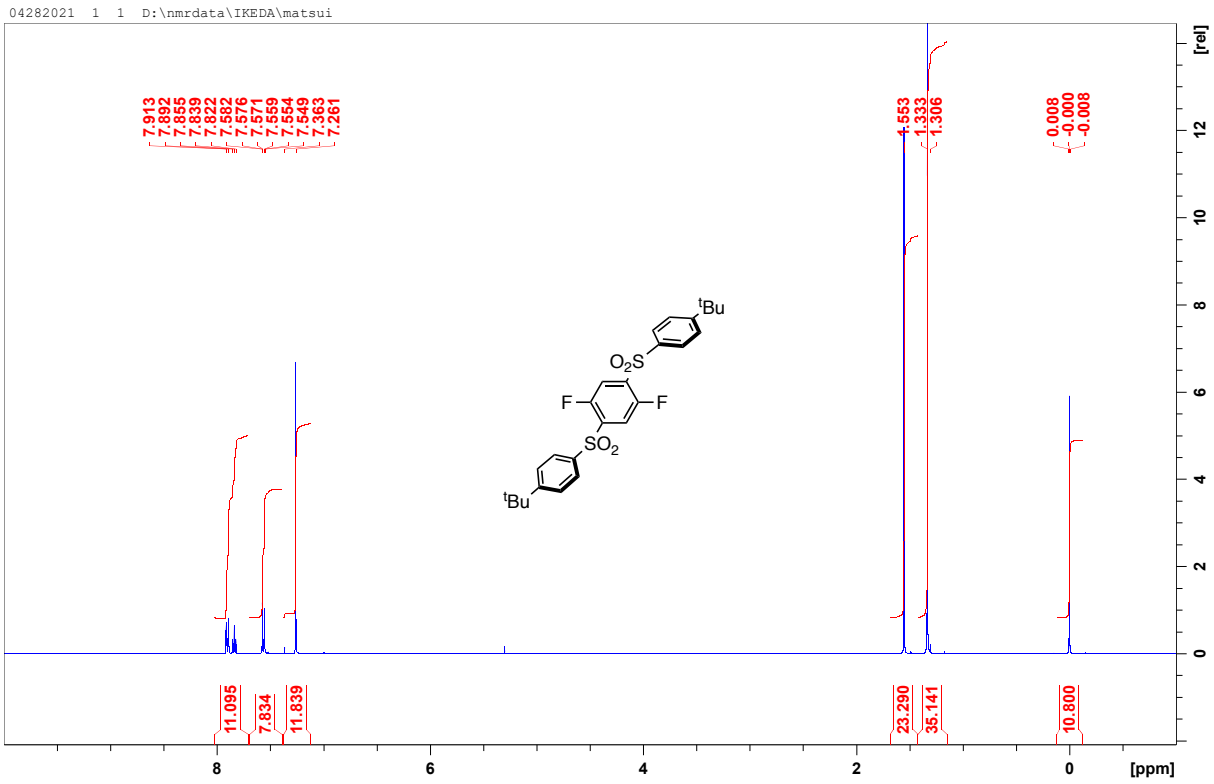

Fig. S15. ^{1}H NMR spectrum of **2** (400 MHz, $CDCl_3$).

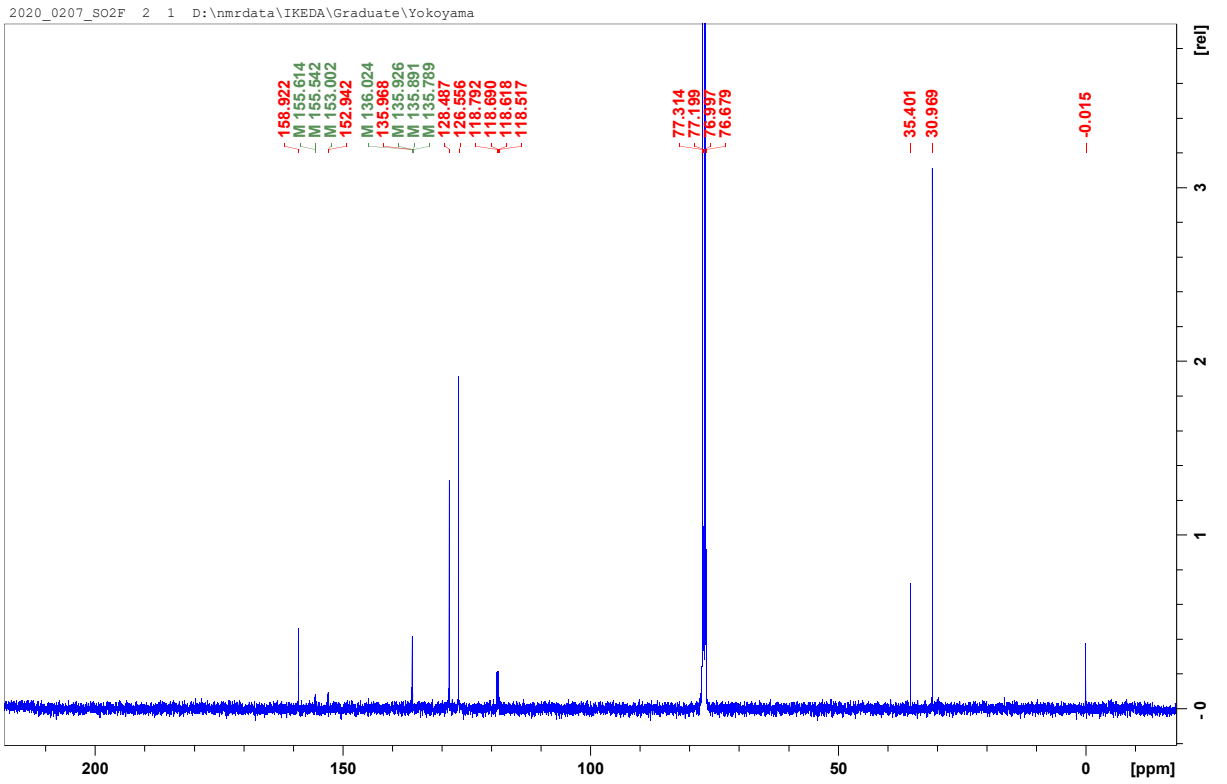

Fig. S16. ^{13}C NMR spectrum of **2** (100 MHz, $CDCl_3$).

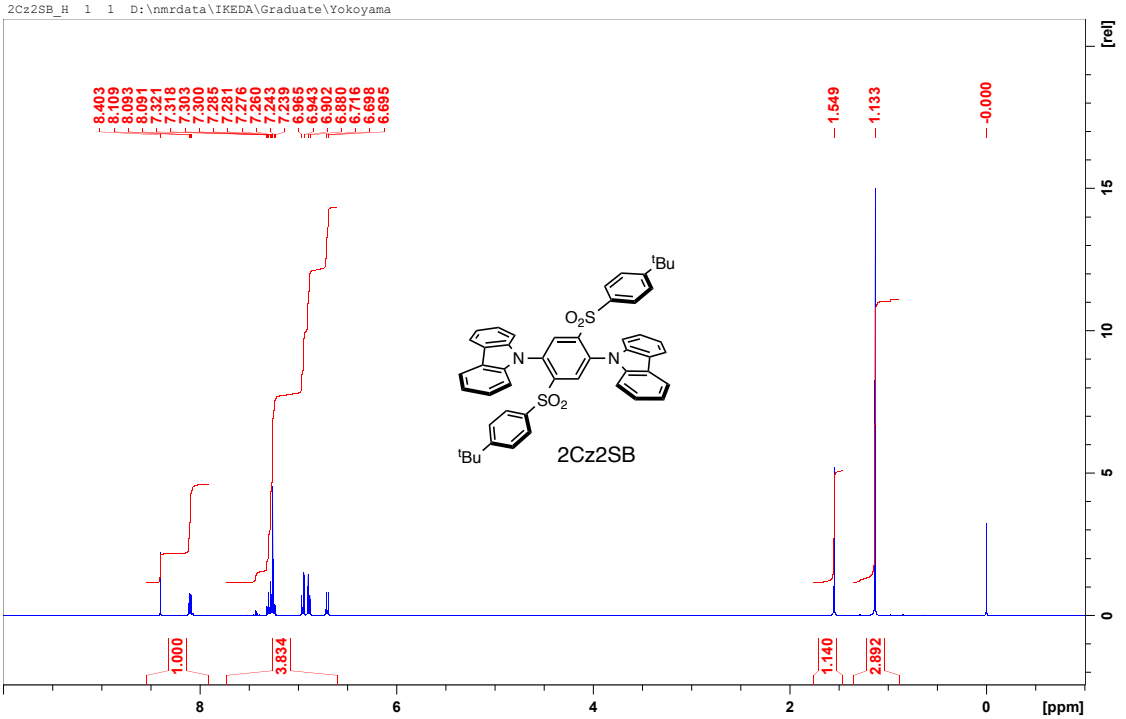

Fig. S17. ^{1}H NMR spectrum of 2Cz2SB (400 MHz, $CDCl_3$).

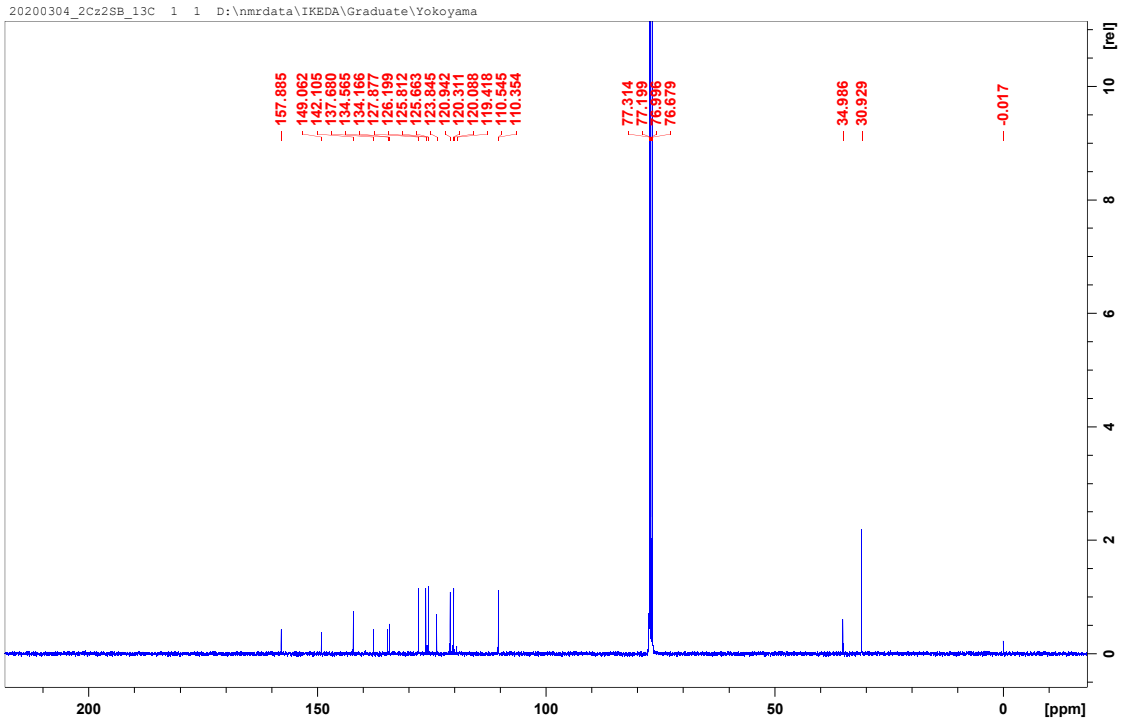

Fig. S18. ^{13}C NMR spectrum of 2Cz2SB (100 MHz, $CDCl_3$).

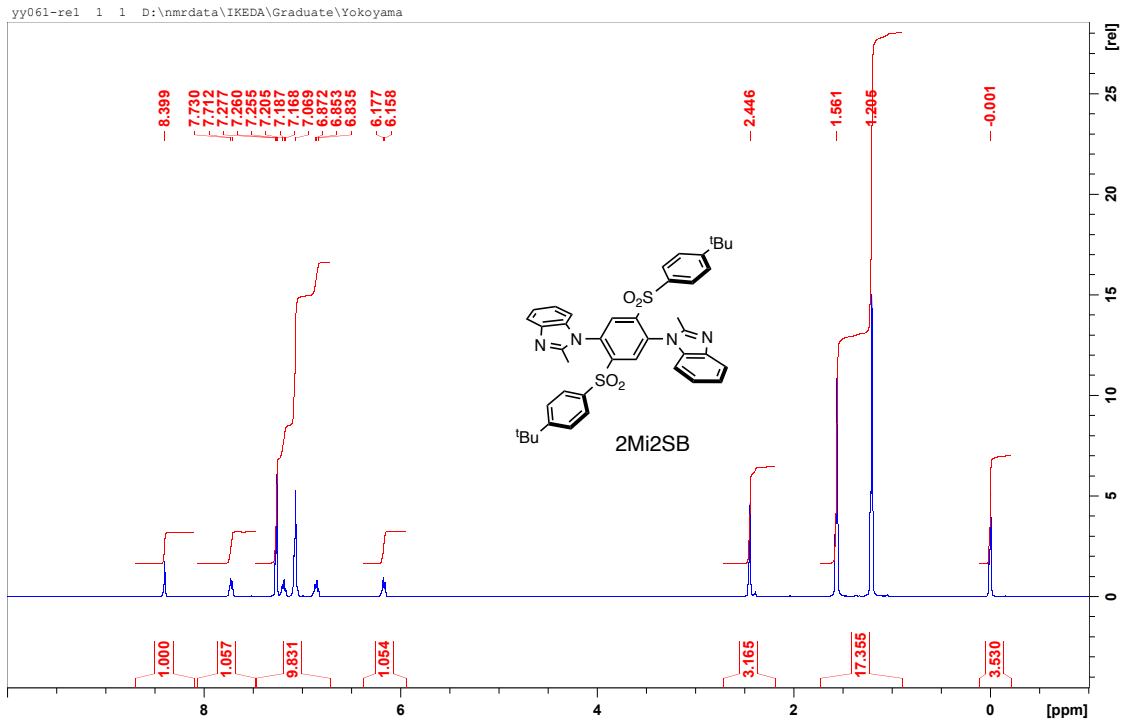

Fig. S19. ^{1}H NMR spectrum of 2Mi2SB (400 MHz, $CDCl_3$).

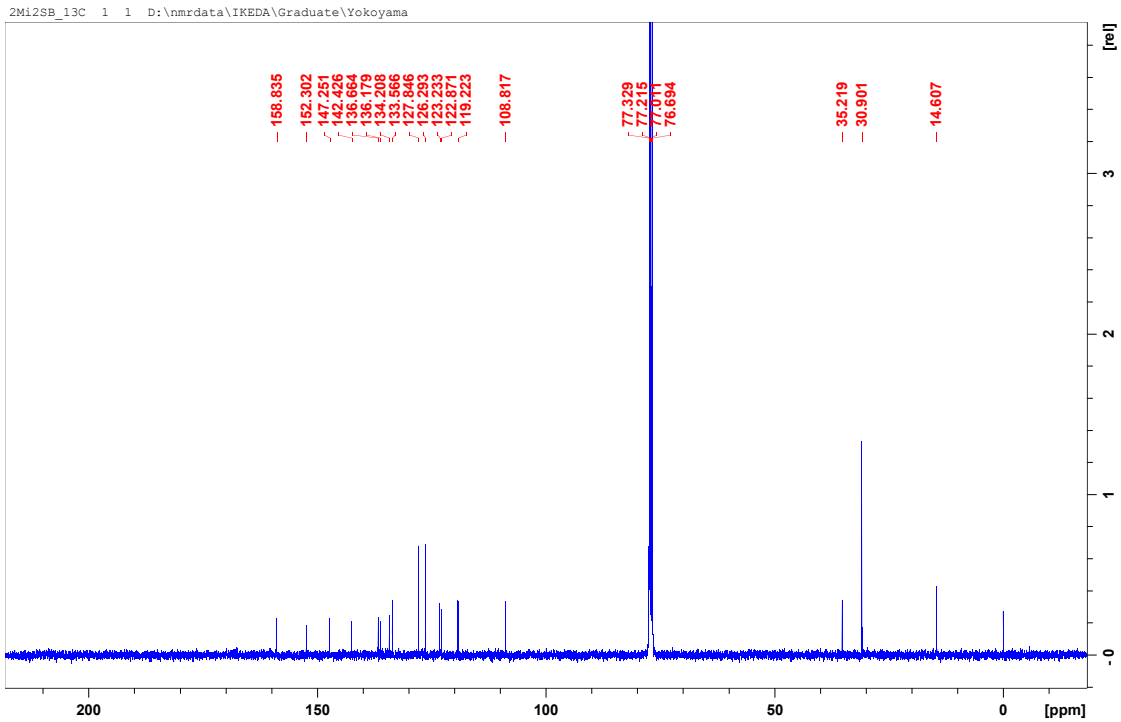

Fig. S20. ^{13}C NMR spectrum of 2Mi2SB (100 MHz, $CDCl_3$).

(EOF)